Biological and Morphological Effects of Apatite Kinds (Sheep/Synthetic) on MgO Reinforced Bone Tissue with Hydroxyapatite Matrix

A. Akilli Ari[a,*], H. Evlen[b] and N. Demirkol[c]

[a] *Mechanical Engineering, Amasya University, 05300, Amasya, Turkey*
[b] *Industrial Design Engineering, Karabuk University, 78050, Karabuk, Turkey*
[c] *Department of Ceramic, Kocaeli University, Kocaeli, 41140, Turkey*

Received: 30.12.2021 & Accepted: 20.04.2022

Doi: 10.12693/APhysPolA.142.201 *e-mail: aysu.akilli@amasya.edu.tr

In this study, the biological and morphological structure of the bone tissue of hydroxyapatite produced from synthetic and natural bone was investigated. For this purpose, a three-dimensional bioprinter was designed and manufactured. For the production of bone tissue scaffolds, 10 wt% magnesium oxide added to synthetic hydroxyapatite and sheep hydroxyapatite bioink composites were prepared. The rheological analysis of the prepared bioinks was carried out. With the produced three-dimensional bioprinter, $10 \times 10 \times 2$ mm^3 bone tissue scaffolds were bioprinted. Calcium chloride was used to form connective tissue between layers. 4 weeks of in-vitro bioactivity tests were applied in order to observe the behavior of the produced bone scaffolds and the formation of apatite in the body. After the bioactivity tests, scanning electron microscope and energy dispersive spectrometry analyzes were performed. In addition, a 3-4,5-dimethyl-thiazolyl-2,5-diphenyltetrazolium bromide test was performed in the laboratory environment of the bone tissue scaffolds. In this test, cytotoxicity analyses and cell counts were performed by fibroblast and osteoblast cell loading. Viability and cell proliferation were observed using the phalloidin staining method, and comparisons were made between the mixtures. As a result of the study, the printing ability of both bioinks on the three-dimensional bioprinter was successful. Thus, the bone tissue scaffold of the printed bioink was produced in the desired porous structure. Apatite formations were observed in the scanning electron microscope images of the bone tissue scaffolds that were kept in artificial body fluid for 4 weeks. In the cell culture analysis performed at the last stage with cell viability analysis, the continuation of cell viability was promising.

topics: magnesium oxide, bioink, bone scaffold, cell culture

1. Introduction

The three-dimensional (3D) bioprinting technique is the process of producing functional tissue structures and organs from digital 3D models using bioinks. In this process, cell-loaded bioinks or scaffolds with subsequent cell cultivation are used [1,2]. Also, the 3D bioprinting method has the potential to produce automation, high precision, sophisticated, biomimetic tissue structures [3].

Whether or not an artificial scaffold shows the expected performance is evaluated according to criteria such as the compatibility of the scaffold with the body without causing toxic effects, the number of viable cells and its gradual increase. Obtaining a successful cell scaffold with all these features depends on the biomaterial from which the scaffold is produced and the correct production parameters. Many studies are carried out to achieve the desired accuracy of parameter in the artificial bone scaffolding studies with bioprinters. Studies aimed at determining the optimum printing parameters require a variety of printing parameters defined for a bioprinter. In designed and manufactured bioprinters, the scaffold pore in microns should be created for bone tissue printing. These pores affect the ability of the scaffold to retain cells during cell culture. In addition, features such as syringe printing pressure, speed and movements of the printer head, the needle (printer tip) inner diameter [4–6], ensuring air circulation of the environment, disinfection of the environment and the scaffold with UV, and a mechanism spraying the cross-link solution to the scaffolds are used in scaffold printing. These are the most important features to look for in a printer. Therefore, it is necessary to determine the optimum printing parameters to ensure successful printing when printing bioink. Different printing parameters bring different results and enable the desired result to be achieved [7]. Tapered needles are the most suitable needle structure to obtain different cylindrical shapes and to achieve high printing speeds [8]. While the syringe causes the bioink to spread on the tissue scaffold tip when too close to

the tray during printing, it also causes the bioink to flow discontinuously when far from the tray. Also, a layer height equal to the diameter of the syringe should be used to ensure good bioprinting between optimum values [4]. In the literature review it was seen that a needle with a printing speed of 4mm/s and a larger inner diameter was used to obtain more accurate prints with a higher cell viability. As the inner diameter of the needle increases, the pressure decreases, and the probability of cell death also decreases [5].

Biodegradable bone implants have an important place in bone defect repair. An ideal bone implant is defected inversely with the new bone formation [9]. A good bioink prepared for tissue scaffolding should consist of materials that ensure that the scaffold structure is durable, biodegradable, biocompatible, and has a high cell adhesion rate. Among the most preferred bioink materials are natural polymers such as collagen, chitosan, hyaluronic acid, silk, gelatin, chitin, cellulose and alginates, synthetic polymers containing polyesters, polyurethanes, and thermoplastics (PLA, PLGA, PCL, PU, PVA, ABS, PEEK, Poloxamine etc.), and combinations of metallic materials such as iron (Fe), manganese (Mn), calcium (Ca), magnesium (Mg), titanium (Ti), and graphene [9].

In the production of bioprinted scaffolds, literature studies show that the prepared bioink and binding agents as well as printing parameters affect the quality of bioprinting. In this study, bioink prepared by using 3% by weight sodium alginate in an 18–20°C environment was used. The syringe tip diameter is 200 μm, the printing speed is 8 mm/s, the printing pressure is 0.2 bar, and calcium chloride ($CaCl_2$) is chosen as the scaffold binder material. The prints were made under these conditions and successful results were obtained [10].

Alginate is a common component of bioinks because of its well-defined ionic crosslinking mechanism and tunable viscoelastic properties. In extrusion-based 3D printing of alginate inks, additives such as gelatin and pluronic and pre- or post-press crosslinking processes are required for extrusion. Researchers studied the fiber printability and the monitoring of the internal microstructure at different time points of ink gelling. They also performed a well-defined set of rheological tests to obtain pre-ink properties in the 3D printing process. This new perspective allowed reactive 3D printing of alginate fibers with predetermined properties, without post-extrusion crosslinking steps and additives [11].

Hydroxyapatite (HA) is one of the widely used biomaterials in medical implants due to its close chemical similarity to the natural bone in the human skeleton, mineral components in the dental system and crystal structure, rapid bone formation and positive effects on the healing around damaged areas in the body [12]. Natural calcium HA, which is the main phase in bone structure, has a porous lattice of not less than 50% in cortical bones and over 75% in trabecular bones. The pores in human bones range in size from 100 to 500 μm and are filled with natural bone marrow [13].

Researchers in the literature prepared a poly(lactic-co-glycolic acid) (PLGA)/MgO-alginate core-shell microsphere system. As a result of the study, they emphasized that MgO effectively neutralizes the acidic degradation products of PLGA [14]. In another study, MgO was reinforced into poly(3-hydroxybutyrate-co-3-hydroxyvalerate) to fabricate composite scaffolds. As a result of the immersion tests, it was stated that the pH value was maintained at the level of 7.5 during the 4-week soaking period [15]. Researchers combined a biodegradable polymer (PLGA) with a bioceramic material (β-tri calcium phosphate) to prepare bone scaffolds using low temperature rapid prototyping technique (LT-RP). Magnesium (Mg), a biodegradable metal, was supplemented to improve the mechanical strength of the scaffolds [16]. Y. Lai et al. [16] performed in-vitro mechanical, degradation, and imaging studies, and in-vivo studies to establish models of segmental ulnar bone defects in New Zealand white rabbits. It was observed that increasing magnesium concentrations increased the scaffold modulus and the compressive strength of young rabbits. However, magnesium supplementation had no effect on the porosity of the scaffolds. The authors emphasized also that the histological analysis showed new bone formation with a better osteogenic effects in the groups with Mg [9].

In this study, the aim was to produce a bone tissue scaffold with better mechanical properties and cell adhesion ability by supplementing sheep hydroxyapatite (SHA) and synthetic hydroxyapatite (CSHA) with sodium alginate ($(C_6H_7NaO_6)_n$) and micron magnesium oxide (MgO). The SHA/MgO and CSHA/MgO scaffolds were produced by micro-extruded fused deposition modeling (FDM) method. Thus, it became possible to interfere with the porous size of the scaffold and the scaffold occupancy rate. The mechanical properties, biocompatibility, and biodegradability of the scaffolds were examined and viable cell counting was performed by cell loading.

2. Material and method

2.1. Material

In the study, CSHA was obtained from Nanografi Nano Technology company (purity of 99.5%, size of 40–50 μm). SHA (grain size of 10 μm) was obtained by calcining and burning sheep bones in an electric oven at 350°C for 2 h and keeping them in the oven at 750°C for 4 h to form the apatite structure. Then it was ground and dried in an oven at 105°C and made ready for use [17]. SHA and CSHA were used as the main material. Mixtures were prepared by adding 10 wt% MgO (obtained from Nanografi

TABLE I

Material and weight percent [%] of the mixture.

Bioink codes	Biomaterials	Mixture content [% w/v]
CSHAB	[CSHA + 10 wt% MgO + $(C_6H_7NaO_6)_n$]	7.4% w/v, [CSHA + 10 wt% MgO] 3.8% w/v, [$(C_6H_7NaO_6)_n$] 25 mL distilled water
SHAB	[SHA + 10 wt% MgO + $(C_6H_7NaO_6)_n$]	7.4% w/v, [SHA + 10 wt% MgO] 3.8% w/v, [$(C_6H_7NaO_6)_n$] 25 mL distilled water

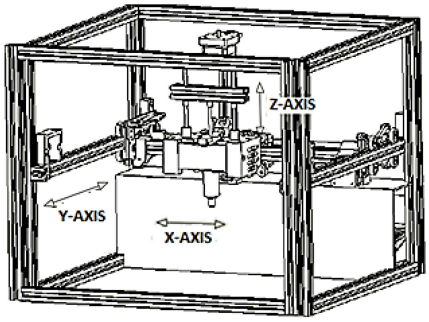


Fig. 1. The designed and manufactured bioprinter model.

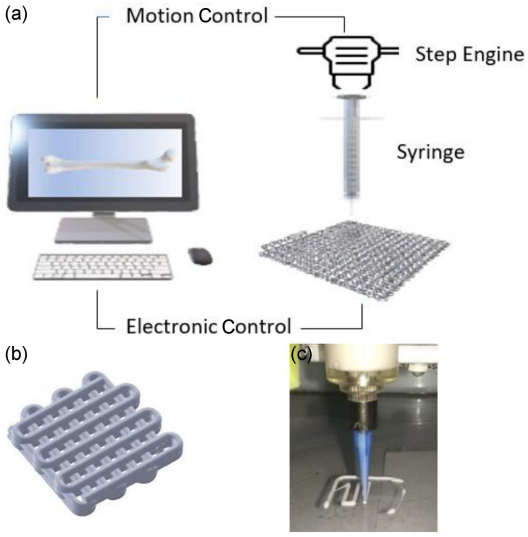


Fig. 2. (a) Printing process, (b) CAD model of bone tissue scaffold, and (c) bioprinter printing.

Nano Technology company, purity of 99.99%, size of 325 mesh) to this biomaterial. Two different bioinks were obtained by adding $(C_6H_7NaO_6)_n$ (purchased from Alfasol company) and distilled water to the mixtures thus prepared.

2.2. Method

2.2.1. Prototyping parameters in bioprinter

In order to produce cell scaffolds on a 3D bioprinter (Fig. 1), the prototype of which was produced in the previous work of the authors [3], a 3D model of the scaffold structure was drawn using computer-aided design programs. In order to establish a connection between the printer and the 3D model, and to determine the model's printing parameters, the model was saved in *.stl format and sent to the program where the print settings are made. Printing parameters were determined by the program [3, 18].

The printing parameters of the bioprinter were kept the same in the bioink mixtures. These parameters were applied as printing speed 400 mm/min, layer thickness 0.25 mm, nozzle diameter 0.41 μm, bone tissue scaffold dimensions $10 \times 10 \times 2$ mm^3, number of layers two, and printing fill rate 10%.

The production process of the designed bioprinter is shown in Fig. 2a. At this stage, the bone scaffold of a computer-controlled bioprinter was modeled and the values of the printing parameters were entered into the CAM program [19]. The scaffolds were created on the printing table with the help of the bioprinter stepper motors. The CAD model of bone tissue scaffold to be printed is shown in Fig. 2b. The printing of the model transferred to the bioprinter with a syringe is shown in Fig. 2c.

The formed bone scaffold should have a pore size of 100–500 μm suitable to the bone structure [13]. This requirement is one of the most important parameters in bioprinting. Therefore, the printer's extruder is designed to be able to feed in microns. In addition, the inner diameter of the syringe to be used during printing affects the speed of the bioink in the printing. The viscosity of the bioink should be determined according to the syringe tip to be used. Preliminary tests were carried out to determine the parameters of the bioprinting process. In preliminary tests, the rheological properties of the bioink with the best fluidity and printing were carried out.

2.2.2. Bioink preparation

In order to prepare the scaffold printing, biomaterials were selected from materials that can form bone tissue on which cells can proliferate and that can be easily printed [20]. Additive alginate bioinks are used to print a wide variety of cell types [21]. alginate systems are also used in stem cells, fibroblasts, neurons, and hepatocytes, as their versatility and mechanical properties are adaptable [22].

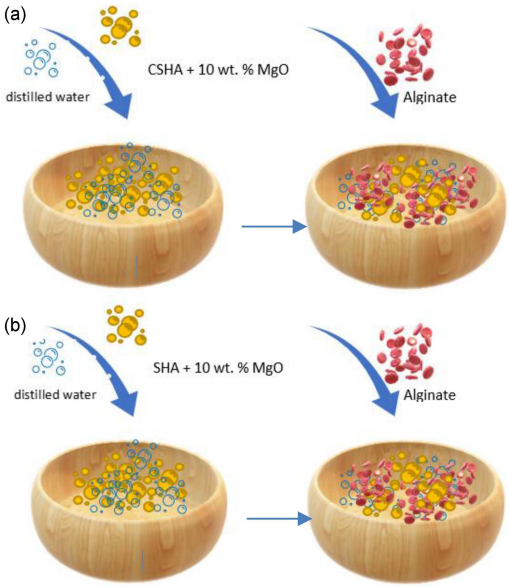


Fig. 3. Schematic representation of the preparation of CSHAB (a) and SHAB (b).

Considering the ease of manufacturing of alginate systems, they are used for their effect on cell growth and behavior [21, 23]. Calcium chloride ($CaCl_2$) was used as a binder after printing due to alginate additive. The mixture content [% w/v] codes of the bioink and biomaterials of the prepared bioinks are given in Table I.

In CSHAB, 10 wt% MgO was added to the CSHA base material. For the new bioink mixture, 7.4% w/v of this mixture was added. The bioink was prepared by adding 3.8% of the mixture to sodium alginate and 25 mL of distilled water. In SHAB, the same amount of mixtures were made, but SHA was used instead of CSHA. In this way, two different bioinks were obtained.

As shown in Fig. 3, the mixtures were put in a container to which pure water was added, and mixed with a magnetic stirrer at 60°C for 90 min. The alginate was added to the mixture and it was mixed for 120 min until a consistency was obtained. When the mixture reached the desired consistency, the bioink was taken into the syringe and made ready for printing.

2.2.3. Rheological behavior

Rheological studies were analyzed using the Malvern/Gemini II rheometer device by the Hitit University Scientific Research Projects Coordinatorship (HUBTUAM). As experimental parameters, a constant temperature of 25°C and parallel plates of 40 mm diameter with a 4° conical angle were used. The solutions were allowed to reach equilibrium temperature for 1 min before the experiments were carried out, and the bioink measurements were made at a cut-off speed of 0.000–1000.000 s^{-1} and a frequency of $f = 1.5$ Hz. The storage modulus (G') is determined by the ratio of the elastic stress to strain, and G' gives information about the elastic property of the material and how much energy is stored in the material structure. The lost modulus (G'') is the ratio of the viscous stress to strain and gives the viscous properties of the material and the energy lost from the material structure over a cycle [24, 25]. Viscosity [Pa s], shear rate [s^{-1}], storage modulus (G'), and loss modulus (G''), tan(δ) values were compared in the test results.

TABLE II

Chemicals used in the preparation of 1.5X SBF and their amounts (1000 ml) [30].

Material	Quantity
NaCl	11.994 g
$NaHCO_3$	0.525 g
KCl	0.336 g
$K_2HPO_4 \cdot 3H_2O$	0.342 g
$MgCl_2 \cdot 6H_2O$	0.458 g
1.0M HCl	60 ml
$CaCl_2$	0.417 g
Na_2SO_4	0.107 g
Tris (Hydroxymethyl)	9.086 g

2.2.4. Formation of apatite in simulated body fluid

Artificial body fluid (SBF) solutions cause the formation of apatite calcium phosphate on polymers, metals and ceramics [26]. A static bioactivity test was applied to generate apatite [17]. In this study, this method was chosen because the accumulation of calcium ions and the formation of a phosphate layer on surfaces with awaited bone tissue scaffolds in SBF are important steps in the growth of bone-like apatite [27].

In Table II, the chemicals used to prepare 1.5X SBF and their amounts in 1000 ml are given. Controls for this apatite formation in SEM images were made before placing it in the SBF solution and during 4 weeks when it was stored there.

Bone tissue scaffolds formed from CSHAB and SHAB were prepared in SBF solution, and the immersion method was used for 4 weeks. In the SBF setup in Fig. 4a, the bottle was filled with SBF and the bone tissue scaffold was immersed. It was then kept there at 36°C for 4 weeks. During the waiting period, SBF solutions containing the bone scaffold samples were changed every three days and refreshed. This is shown in Fig. 4b. It was observed that there was no deterioration in the shape of the bone tissue scaffold after SBF with 10% occupancy that it was kept in for 4 weeks.

2.2.5. SEM–EDS

In order to visualize the formation of apatite clusters of bone scaffolds, SEM and EDS images were taken with Nova NanoSEM 450 device by the HUBTUAM.

2.2.6. MTT cell viability analysis

A bone scaffold was formed from each mixture. The cell culture cytotoxicity/cell viability test of these scaffolds was carried out by the HUBTUAM.

The L-929 (mouse subcutaneous connective tissue) cell line was used for the study. The samples were extracted. The extraction process was performed in 10% serum cell culture medium at 37°C in a water bath oscillating at 50 rpm for 24 h. Afterwards, the extraction was terminated and the obtained extract was used within 24 h.

All data were presented as mean ± standard deviation (SD).

Statistical analysis was performed using the one-way analysis of variance (ANOVA) to test for significance.

2.2.7. Cell culture

The L929 Mouse Fibroblast cell line was used for cell culture and WST-1 Cytotoxicity/Cell viability assay. These procedures were performed at Kocaeli University Stem Cell Center using a Leica DMI SP8 Confocal microscope. Cells were reproduced by culturing under sterile conditions. It was investigated by fluorescence techniques that the cells did not contain mycoplasma. Cells were cultured under the condition of 37°C and 5% CO_2 [28]. The medium in which the cell culture was made consisted of 10% FBS and L-DMEM containing 1% Pen/Strep. For WST-1 analysis measurements, the absorbance values at 450 nm wave size were determined with a spectrophotometer. Phalloidin evaluation was performed on 3D samples taken by confocal microscopy from the cell seeded and fixed sample. Tissue follow-up was performed on the fixed samples, and the paraffin sections were taken with a microtome. After deparaffinization processes, samples were fluorescently stained for phalloidin staining.

3. Results

The viscosity, shear rate, G'', G' and $\tan(\delta)$ values of the prepared bioink were determined with a rheometer device. In Fig. 5, it can be seen that the viscosity decreases with time. A similar increase and decrease is observed in the viscosity values

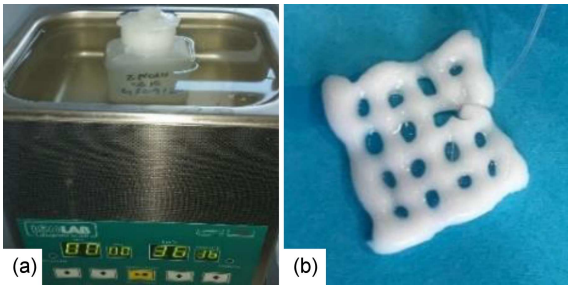


Fig. 4. (a) SBF experimental setup, (b) bone tissue scaffold image after SBF.

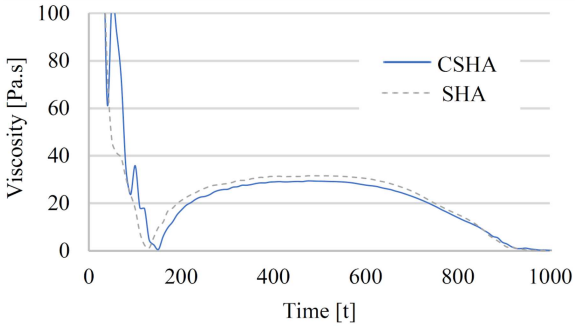


Fig. 5. Density [Pa s] vs time t [s] of rheological result plots.

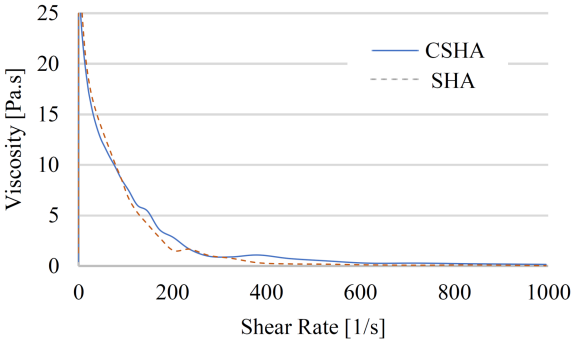


Fig. 6. Density [Pa s] vs shear rate [1/s] of rheological result plots.

of CSHAB and SHAB. It is seen that the viscous increases in the 200–350 s time interval are at a similar rate. The viscous value, which increased in the 350–600 s time interval, changed in parallel with each other as the time increased. If the comparison is made at 600 s, one noted that the CSHAB (27.546 Pa s) and SHAB (30.367 Pa s) groups showed viscous behavior ($G'' > G'$). There is a decrease in viscosity in the interval of 600–900 s. The prepared CSHAB and SHAB mixtures have viscosity values close to each other.

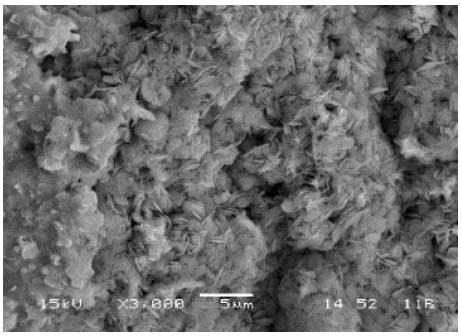
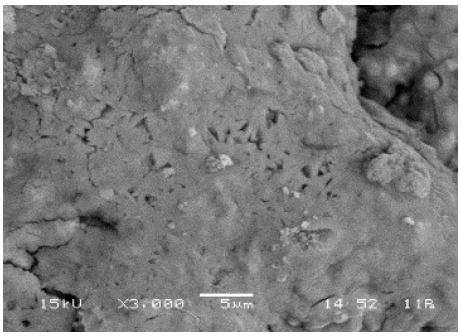
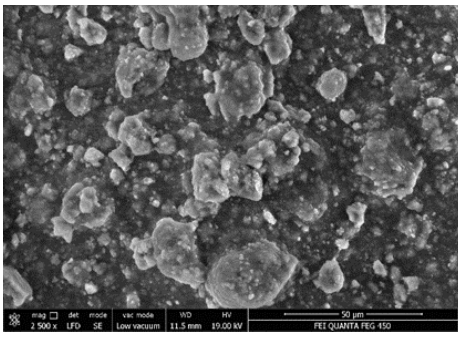
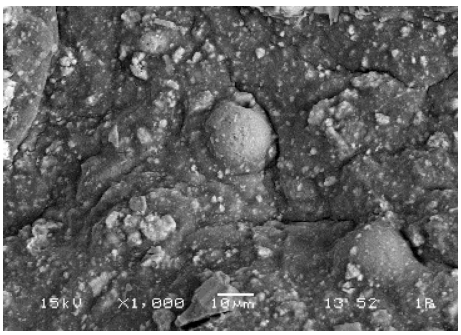
In Fig. 6, CSHAB and SHAB show similar values. The viscous and shear rate of bioinks act inversely related to each other, namely as the viscosity decreases, the shear rate increases. The share rate values at the 20 Pa s viscosity were 20.292 s^{-1} in CSHAB and 23.575 s^{-1} in SHAB. These results showed that the density of bioink, printed at a certain speed and temperature, decreased, but the density was not affected by shear stress.

In Fig. 7, it is seen that when the bioinks are compared with each other, they show viscous behavior because the loss module G'' is larger than the storage module G'.

The dominance of G'' means that the printed ink behaves like a liquid with not enough G' to hold its shape [30]. Thus, if the viscosity of the bioink is too high, it causes the blockages in the syringe tip and

TABLE III

In-vitro bioactivity SEM images of bone tissue scaffolds without SBF and stored in SBF for 4 weeks (5 μm).

Holding time [week]	CSHAB	SHAB
without SBF		
4 weeks		

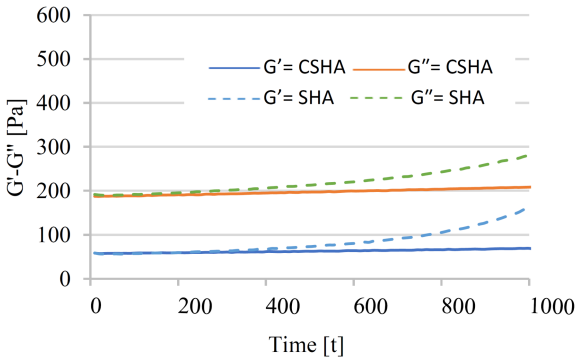


Fig. 7. The storage module G'' and loss module G' [Pa] vs time t [s] of rheological result plots.

the bioprinting process continues in an uncontrolled manner. When very low viscosity bioinks are used, the desired hydrogels cannot be obtained [31]. If the diameter of the syringe tip is wider, the flow rate of the bioink increases. This leads to the closure of the pores in the structure [32]. In order to avoid these problems, the syringe tip diameter was taken as small as 0.41 mm. In addition, the alginate added to the bioink can form a gel in the presence of $CaCl_2$ in order to keep the bioink structure together and reduce the flow of the material [33]. Thus, in order to preserve its shape at the time of printing, $CaCl_2$ was added to the bone scaffold to preserve its shape.

The viscous part with respect to the elastic part tangent is represented with $\tan(\delta)$. The lag between the stress and strain curves is known as the $\tan(\delta)$ angle, where δ reflects the predominance of the elastic (small values) or viscous (high values) behavior of the sample [34]. In Fig. 8, CSHAB is $\tan(\delta) = 3.24$ and SHAB is $\tan(\delta) = 3.37$ in the 20–30 s time interval. The lag angles of the bioinks showed similar values over time. When $t > 30$ s, while the delay angle of CSHAB continues at the same rate, the values in SHAB decrease.

Bone scaffolds were characterized using SEM to visualize the formation of apatite clusters. As a result of SEM analysis of bone tissue scaffold samples kept in SBF for 4 weeks, it is observed that an apatite layer is formed on the surface of all samples. However, no apatite structure was observed in the original tissue scaffolds not kept in SBF. In-vitro bioactivity images of apatite clusters are given in Table III. They are SEM images of the bone tissue scaffolds of the CSHA bioink (CSHAS) and SEM images of the bone tissue scaffolds of the SHA bioink (SHAS) without SBF and with SBF for 4 weeks. When the images of CSHAS and SHAS without SBF are examined, it is seen that there are no apatite clusters at the desired density on the bone tissue scaffold. When the 4 weeks SEM images are examined, it is seen that apatite formation in the bone tissue scaffold of CSHAS (Ca 5.96 wt%) decreased compared to the bone scaffold of SHAS (Ca 176.15 wt%). The Ca/P ratio is

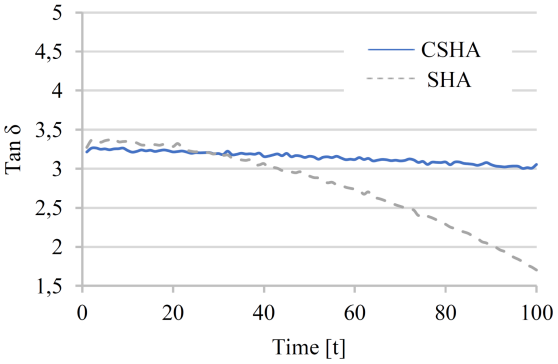


Fig. 8. The dependence tan(δ) vs time [t] of rheological result plots.

TABLE IV

EDS spectra of the scaffold end of 4 weeks

Element	CSHAS		SHAS	
	Weight [%]	Atomic [%]	Weight [%]	Atomic [%]
C K	31.92	41.92	61.90	19.586
O K	49.11	48.41	148.74	42.330
Na K	4.45	3.05	59.69	5.445
P K	7.23	3.68	159.15	10.148
Cl K	1.33	0.59	73.82	5.344
Ca K	5.96	2.35	176.15	15.807

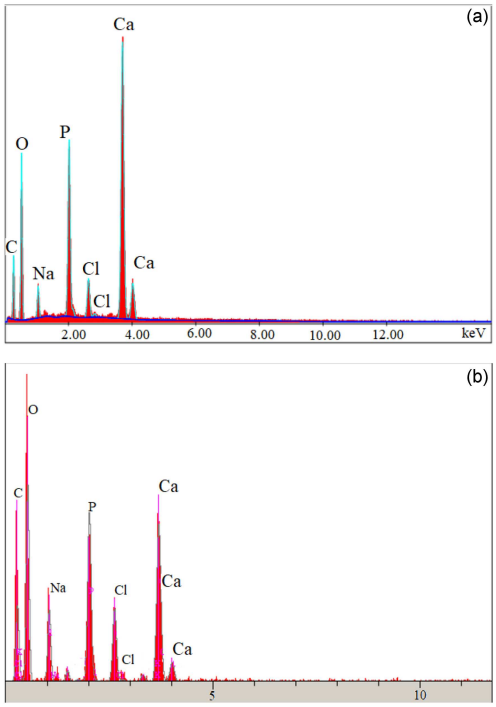


Fig. 9. EDS spectra of the samples that were kept in SBF for 4 weeks for (a) scaffold of CSHAS, (b) scaffold of SHAS.

calculated from the elemental composition (atomic percentages) obtained from EDS. These are calculated as CSHAS (0.63) and SHAS (1.55), see Fig. 6, Table IV) [24, 35, 36, 37].

In qualitative evaluation, cells were seeded in 96-well plates and expected to become confluent. Then, they were incubated in an oven device at 37°C, 5% CO_2 for 24 h. After incubation, they were exposed to negative-positive control and sample extracts. The cells were then examined microscopically.

In the quantitative evaluation, 80% confluence was achieved in the incubated bone scaffold. The cells were then exposed to 1/1 to 1/64 dilutions of the sample extract for 24 h. At the end of the process, MTT prepared as 1 mg/mL was added to the wells, and the plates were kept in an oven device at 37°C, with 5% CO_2 for 3 h. The experiment was terminated by adding isopropyl alcohol to the wells. Viability percent values were calculated by measuring the color change in the plates in the spectrophotometer. In the spectrophotometer measurements, absorbance values were determined at a wave size of 570 nm.

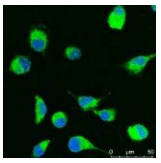
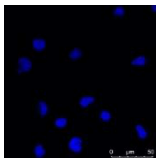
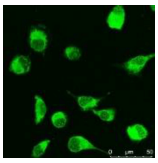
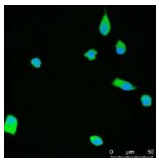
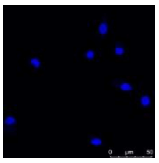
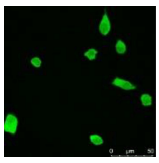
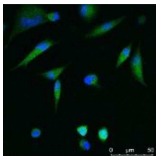
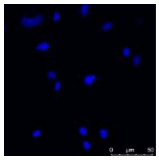
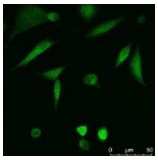
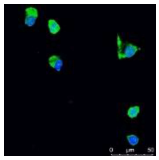
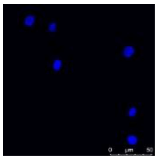
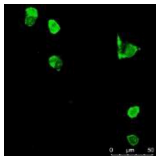
For quantitative evaluation, the standard "TS EN ISO 10993-5/ October-2010- EK-C MTT Cytotoxicity Test" was used, and the results were evaluated statistically. It is seen that the results obtained from the negative and positive controls used in the tests meet the test validity criteria. As shown in Fig. 7a, it was determined that the L929 cell line had no in-vitro cytotoxic effect since there was more than 70% cell viability in CSHAS and SHAS [38]. As in Fig. 7b, it was observed that each experimental sample was not cytotoxic in osteoblast cells [39].

MTT analysis was performed at 24 h. The statistical significance was defined as 0.05. There are statistically significant differences in bone scaffolds in fibroblast cell line concentrations ($p < 0.05$). There are no significant differences in osteoblast cell line concentrations on the CSHAS scaffolds ($p > 0.05$). There are statistically significant differences in SHAS scaffolding. Since the test acceptance criteria specified in the standard are met, it is appropriate to use bone tissue scaffolds in in-vivo and in-vitro studies.

DAPI staining shows cell nucleus (blue), phalloidin staining shows viable cell (green), and MERGE shows a combination of both images [40]. The scale of confocal images is 50 μm. Bone tissue CSHAS and SHAS were cultured for 12 and 36 h using L929 Fibroblast cells, as shown in Table V [41]. Comparing the MERGE images of cultured scaffolds, the DNA image appears to be highly fluorescent in the cells, nuclei, and intracellular at 36 h of culture [42]. The characteristic feature of osteogenic differentiation's initiation, which is the bone-forming cells in the scaffolds, is the cross-linked web-like structures [24, 29, 43]. It is seen that bone tissue similarity has increased in tissue CSHA [44].

TABLE V

Images of the bone tissue CSHAS and SHAS using L929 Mouse Fibroblast cells, taken by confocal microscopy at 12 and 36 h.

	CSHAS			SHAS		
	MERGE	DAPI	PHALLOIDIN	MERGE	DAPI	PHALLOIDIN
12 hour						
36 hour						

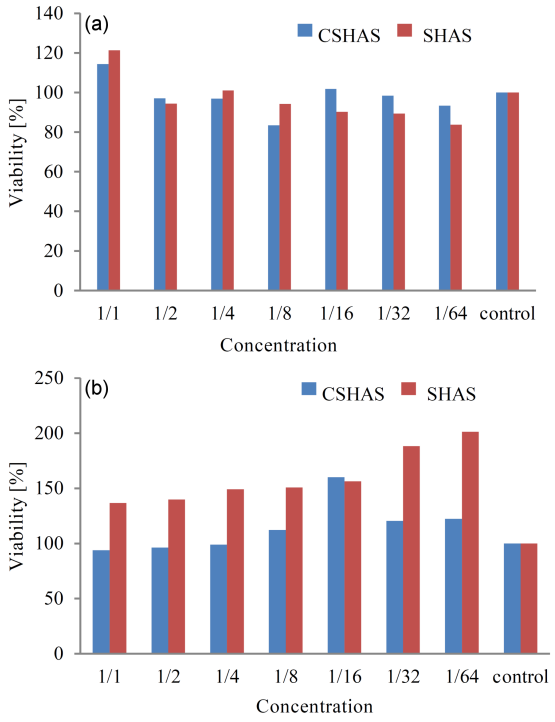


Fig. 10. Graph of viability [%] in concentration dependent of (a) L929 cell line (b) osteoblast cell line.

4. Discussion

The usability of the printing parameters of the designed and manufactured bioprinter has been confirmed by this study. CSHA, SHA, MgO, and alginate were used, which are biomaterials compatible with the body. Thus, 10 wt% MgO has been added to CSHA and SHA. By adding alginate and distilled water to this mixture, two different bioinks were obtained. The viscosity of the bioprintable bioink was measured with a rheometer device. When the rheometer results were examined, CSHAB and SHAB showed similar viscous behavior. After the scaffolds of bone tissue had been kept in SBF for 4 weeks, their images were taken by SEM. When examining SEM images, clustering was observed in the apatite density of the bone tissue CSHAS.

MTT test was applied to the bone tissue scaffold to determine whether there is a toxic effect on the body. In the MTT test, bone tissue CSHAS and SHAS were examined microscopically by keeping them in the L929 mouse cell line and Osteoblast cell line for 24 h. For quantitative evaluation, TS EN ISO 10993-5/ October-2010- EK-C MTT Cytotoxicity Test standard was used. Since more than 70% of cells proliferated in bone tissue CSHAS and SHAS, it met the validity criteria. Preliminary experiments at the in-vitro level cannot be fully equivalent to in-vivo studies. However, they provide valuable information on the potential molecular mechanism of action of compounds in cells and are the basis for further experiments in this direction. Thus, they were deemed appropriate to be used in laboratory studies. Confocal microscope images were obtained to determine cell viability with the phalloidin staining technique, which is the last step. The cell culture results of bone tissue CSHAS and SHAS after 12 and 36 h were taken. At the end of 12 h, the cell viability of the bone CSHAS is higher than the cell viability of SHAS. At the end of 36 h, osteogenic differentiation of the bone tissue CSHAS started, and cross-linked mesh-like structures were formed.

5. Conclusions

As a result of the experiments in this study, results similar to the bone cell network of the bone tissue CSHAS were obtained. It was concluded that more promising results would be obtained in in-vitro and in-vivo experiments by developing bioink. This study revealed results that will give additional insight to many studies in the literature.

Acknowledgments

The authors thank the Scientific Research Project Department of Karabuk University for financial support as part of the KBÜBAP-17-DR-303 project.

References

[1] S. Vijayavenkataraman, W.C. Yan, W.F. Lu, C. Wang, J.Y. HsiFuh, *Adv. Drug Delivery Rev.* **132**, 296 (2018).

[2] M. Wang, H. Li, Y. Yang, K. Yuan, F. Zhou, H. Liu, T. Tang, *Bioact. Mater.* **6**, 1318 (2021).

[3] A. Akıllı, H. Evlen, in: ISIDE 2nd Int. Symposium on Industrial Design & Enginnering, Turkey 2017, p. 13.

[4] E. Sodupe-Ortega, A. Sanz-Garcia, A. Pernia-Espinoza, C. Escobedo-Lucea, *Materials* **11**, 1402 (2018).

[5] H. Honaryar, J.A. LaNasa, E.C. Loyd, R.J. Hickey, Z. Niroobakhsh, *Macromol. Rapid Commun.* **42**, 2100445 (2021).

[6] X. He, Y. Ding, Z. Lei, S. Welch, W. Zhang, M. Dunn, K. Yu, *Addit. Manuf.* **40**, 101921 (2021).

[7] W. Braeden, J.B. Doyle, *Bioprinting* **8**, 8 (2017).

[8] E.S. Ortega, A. Sanz-Garcia, A. Pernia-Espinoza, C. Escobedo-Lucea, *Materials* **12**, 613 (2019).

[9] M. Singh, S. Jonnalagadda, *Eur. J. Pharm. Sci.* **143**, 105167 (2020).

[10] S. Naghieh, M.D. Sarker, M.R. Karamooz-Ravari, A.D. McInnes, X. Chen, *Appl. Sci.* **8**, 1422 (2018).

[11] S. Lorenzo, M. Tunesi, B. Vangosa, P. Francesco, *Soft Matter* **35**, 8105 (2021).

[12] C.Y. Tan, K.L. Aw, W.H. Yeo, S. Ramesh, M. Hamdi, I. Sopyan, in: *4th Kuala Lumpur Int. Conf. on Biomedical Engineering 2008*, Vol. 21, 2008, p. 326.

[13] A. Pasinli, R.S. Aksoy, *Electron. J. BioTechnol.* **1**, 41 (2010).

[14] Z. Lin, J. Wu, W. Qiao et al., *Biomaterials* **174**, 1 (2018).

[15] C. Shuai, W. Guo, C. Gao, Y. Yang, P. Wu, P. Feng, *Int. J. Bioprint.* **4**, 120 (2017).

[16] Y. Lai, Y. Li, H. Cao et al., *Biomaterials* **197**, 207 (2019).

[17] N. Demirkol, PhD Thesis, Istanbul Technical University, 2013.

[18] K. Thakare, L. Jerpseth, H. Qin, Z. Pei, *J. Manuf. Sci. Eng.* **143**, 014501 (2021).

[19] H. Christina, B. Maria, B. Athina, K. Petros, in: *In 3D Printing: Applications in Medicine and Surgery*, Vol. 2, Eds. V.N. Papadopoulos, V. Tsioukas, J.S. Suri, 2022, p. 195.

[20] S. Gundu, N. Varshney, A.K. Sahi, S.K. Mahto, *J. Polym. Res.* **29**, 1 (2022).

[21] C.C. Piras, D.K. Smith, *J. Mater. Chem. B* **8**, 8171 (2020).

[22] Y. Xiang, K. Miller, J. Guan, W. Kiratitanaporn, M. Tang, S. Chen, *Arch. Toxicol.* **96**, 691 (2022).

[23] Mengjie Xu, Miao Qin, Yizhu Cheng, Xiaolian Niu, Jinlong Kong, Xiumei Zhang, Di Huang, Huanan Wang, *Carbohydr. Polym.* **266**, 118128 (2021).

[24] G. Irmak, Ph.D. Thesis, Hacettepe University, 2019.

[25] S. Bom, R. Ribeiro, H.M. Ribeiro, C. Santos, J. Marto, *Int. J. Pharm.* **615**, 121506 (2022).

[26] G. Ü. L. Canser, S. Mutaf, H. Durmuş, *J. Eng.* **11**, 1139 (2020).

[27] F.E. Baştan, Ph.D. Thesis, Sakarya University 2018.

[28] A.M. Borkowska, M. Nowakowski, J. Miszczyk, E.W. Lipiec, J. Wiltowska-Zuber, K. Rawojć W.M. Kwiatek, *Acta Phys. Pol. A* **133**, 263 (2018).

[29] J. Dong, N. Tumer, N. E Putra, J. Zhu, Y. Li, S. Leeflang, J. Zhou, *Biomater. Sci.* **9**, 7159 (2021).

[30] T. Kokubo, H. Takadama, *Biomaterials* **27**, 2907 (2006).

[31] S. Wust, M.E. Godla, R. Muller, S. Hofmann, *Acta Biomater.* **10**, 630 (2014).

[32] J.H. Chung, S. Naficy, Z. Yue, R. Kapsa, A. Quigley, S.E. Moulton, G.G. Wallace, *Biomater. Sci.* **1**, 763 (2013).

[33] H. Li, S. Liu, L. Lin, *Int. J. Bioprint.*, **2**, 54 (2016).

[34] A. Poulesquen, F. Frizon, D. Lambertin, *J. Non-Crystal. Solids* **357**, 3565 (2011).

[35] C. Cao, P. Huang, A. Prasopthum, A.J. Parsons, F. Ai, J. Yang, *Biomater. Sci.* **10**, 138 (2022).

[36] A. Díaz-Cuenca, D. Rabadjieva, K. Sezanova, R. Gergulova, R. Ilieva, S. Tepavitcharova, *Mater. Today: Proc.* (2022).

[37] R.K. Athira, *Ceram. Int.* **47**, 30051 (2021).

[38] X. Gu, W. Zhou, Y. Zheng, L. Dong, Y. Xi, D. Chai, *Mater. Sci. Eng. C* **30**, 827 (2010).

[39] Ö. Karataş, M.Sc. Thesis, Izmir Institute of Technology, 2014.

[40] Z. Wu, Q. Li, S. Xie, X. Shan, Z. Cai, *Mater. Sci. Eng. C* **109**, 110530 (2020).

[41] A.J. Mohammedamim, H.S. Ahmed, *Eur. J. Mol. Clinic. Med.* **7**, 1 (2020).

[42] F. Otto, in: *Methods in Cell Biology*, Vol. 33, Eds. Z. Darzynkiewicz, H.A. Crissman, Academic Press, 1990, p. 105.

[43] Q. Tang, X. Lib, C. Laia, L. Lig, H. Wuh, Y. Wangd, X. Shia, *Bioactive Mater.* **6**, 169 (2021).

[44] N.B. Allen, B. Abar, L. Johnson, J. Burbano, R.M. Danilkowicz, S.B. Adams, *Bioprinting* **196**, e00196 (2022).